

“Compressed Graphite” Formed During C₆₀ to Diamond Transformation as Revealed by Scattering Computed Tomography

M. Álvarez-Murga,^{1,2} P. Bleuet,³ G. Garbarino,¹ A. Salamat,¹ M. Mezouar,¹ and J. L. Hodeau^{2,*}

¹European Synchrotron Radiation Facility, Grenoble F-38043 France

²Institut Néel, CNRS, BP 166, F-38042 Grenoble Cedex 9, France

³CEA, LETI, MINATEC Campus, 17 rue des Martyrs, 38054 GRENOBLE Cedex 9 France

(Received 21 February 2012; published 9 July 2012)

The collapsing of C₆₀ into polycrystalline diamond has been studied after nonhydrostatic pressurization at ambient temperature using x-ray scattering computed tomography. Using this selective structural probe we provide evidence of concentric coexistence of “compressed graphite” ($d_{00l} \sim 3.09\text{--}3.11$ Å), sp^2 -graphitelike phase ($d_{00l} \sim 3.35\text{--}3.42$ Å), and sp^3 -like amorphous carbon surrounding polycrystalline diamond ($a \sim 3.56\text{--}3.59$ Å). The so-called “compressed graphite” exhibits a collapsed c axis and is textured with disordered layers. This latter phase is better described as a short interlayered carbon phase with buckled sp^2 - sp^3 layers with possible interlayer bonding. Additionally, our 3D maps of phase distribution and of the residual stress retained in the polycrystalline diamond phase support the importance of stressed synthesis conditions for diamond formation.

DOI: [10.1103/PhysRevLett.109.025502](https://doi.org/10.1103/PhysRevLett.109.025502)

PACS numbers: 81.05.ub, 78.70.Ck, 81.40.Vw

The nucleation mechanism of diamond and other hard carbon phases has been subjected to a large amount of experimental [1] and theoretical [2] work. However, the transformation pathways and the high-pressure behavior of these carbon phases are still under debate. The noncatalytic synthesis of bulk polycrystalline diamond (sp^3 hybridization) requires high-pressure (HP)–high-temperature (HT) treatment of the carbon precursors (> 12 GPa and 2000 °C) [1]. Such HP-HT phase transformations involve intermediate steps where carbon polytypes with mixed sp^2 - sp^3 hybridization and with similar densities are formed [1,2]. Alternatively at lower temperature, diamond-like carbon and homoepitaxial diamond films can be synthesized using various metastable deposition methods such as ion beam, sputtering, plasma, pulsed laser, or chemical-vapor [1].

Heterogeneous mixtures of carbon polytypes can be recovered after a quenching process. The type and ratio of the products strongly depend on the structural organization of the starting material [3]. Studies have shown that systems rich in defects (dangling bonds, dislocations, or sp^2 - sp^3 mixed hybridization) favor diamond nucleation and growth [2–4]. At room pressure and temperature carbon atoms in C₆₀ molecules are essentially in a sp^2 hybridized state with some minor sp^3 contribution (disturbed due to the curvature from planar geometry). These molecules are joined by weak Van der Waals interactions and form a molecular solid with average close-packed face-centered cubic (fcc) structure. This makes C₆₀ an excellent starting material for studying the phase diagram of carbon [1] and its subsequent phase transitions as well as preparing novel superhard nanomaterials.

The P - T phase diagram of C₆₀ itself is extremely rich. Low pressures promote $[2 + 2]$ cycloaddition reactions

and subsequent formation of (C₆₀)₂ dimers, linear ($P < 2$ GPa), layered ($P = 2\text{--}8$ GPa) or 3D polymers ($P > 8$ GPa) [5–8]. At higher temperature ($T > 750$ °C), transformation of these polymeric phases into disordered sp^2 -like structures is induced [6–9]. Their mixed hybridization character leads to layer buckling and interlayer bonding and could be a possible explanation for its reported superhard properties [6,7,9].

Contrary to these drastic transformations, at room temperature the stability of its fcc structure has been observed up to 20 GPa under hydrostatic compression [10]. In contrast, nonhydrostatic compression of C₆₀ leads to its conversion into amorphous and polycrystalline diamond [11]. This transition occurs through an irreversible intermediate step ($P \sim 16$ GPa) where an insulating amorphous structure is formed [12,13]. This phase, reported as “collapsed fullerite,” is modeled either as icosahedral carbon clusters [14] or as a sp^3 -rich atomic carbon network [15]. Relative to the static HP-HT treatment, shock compressions generate strong shear stresses and rapid quenching, transforming C₆₀ to diamond at lower P , T conditions (16 GPa, 100 °C) [16]. This is consistent with molecular-dynamic simulations that suggest the transformation pressure to diamond can be reduced with the application of shear stresses [17].

Of the various carbon polytypes a so-called “compressed graphite” phase (CG) has been reported experimentally by a few authors [18–21]. F. P. Bundy and J. S. Kasper [18] showed that oriented graphite leads to the formation of hexagonal diamond above 15 GPa and 1000 °C. However, below 1000 °C they recovered CG ($d_{002} = 3.1$ Å) and attributed this phase to reverted hexagonal diamond. Recently, W. Mao *et al.* [21] obtained an unquenchable superhard compressed graphite phase ($d_{002} = 2.95$ Å) existing in the range of 16–24 GPa formed at ambient temperature. During

the synthesis of polycrystalline diamond from graphite, T. Irifune *et al.* [22] reported the presence of a small amount of CG ($d_{002} = 3.15 \text{ \AA}$) together with a major amount of cubic and hexagonal diamond phases. C. Le Guillou *et al.* [3] also reported shortening of graphitelike interlayer distance ($d_{002} = 3.07 \text{ \AA}$) from treatment of carbon with different structural organizations at 15 GPa and high temperature. This can also be related to the recent work by T. Ferroir *et al.* [23] who reported concentric spatial arrangements of CG ($d_{002} = 3.186 \text{ \AA}$), with ordinary hexagonal graphite ($d_{002} = 3.352 \text{ \AA}$) and hexagonal diamond in a shocked meteorite. Recent theoretical work [24] has proposed a structural model (Z carbon) for the CG phase reported by W. Mao *et al.* [21].

In this Letter, we present our results on recovered intermediate carbon poly(a)morphs. These phases were obtained by quenching, at midprocess, during the formation of diamond from the compression of C_{60} at room temperature. The identification of these intermediate phases and their residual stress state were carried out using a powerful selective structural probe: diffraction and scattering computed tomography (DSCT) [25–28]. Finally, the 3D maps on phase distribution, on the residual stress signature of diamond synthesis and on the so-called “compressed graphite” phase (CG) are discussed.

For this study, nonhydrostatic pressurization was deliberately imposed to promote diamond formation from C_{60} [11,12]. C_{60} powder was filled into a 1 mm pyrophyllite gasket and compressed between slanted sintered-diamond anvils without the use of a pressure transmitting medium. Pressure was increased at a rate of 1 GPa min^{-1} up to 20 GPa and held for 1 hr at room temperature. DSCT was used as a structural selective probe and performed on the recovered sample. DSCT requires a series of maps of the sample at different angular projections [25–28]. This method is nondestructive and using micro-focused X-rays beam it can offer high spatial resolution (μm^3) and low detection limits in phase selectivity, better than 0.1% in volume. The DSCT experiment was performed at beam line ID22 of the European Synchrotron Radiation Facility (Grenoble, France). A high energy (21 keV, $\lambda = 0.5904 \text{ \AA}$) monochromatic beam was focused down to a FWHM of $2.3 \times 1.6 \mu\text{m}^2$ and 276 000 x-ray diffraction patterns (60 rotation steps \times 200 translation steps \times 23 slices) were collected. Typical exposure times for each pattern were 0.2 s. DSCT uses the diffuse scattering for image reconstruction, and not only the diffracted peaks, as in x-ray diffraction computed tomography. Both scattered and diffracted intensities are then used to reconstruct 2D slices and herein a 3D volume. For each reconstructed volume element (voxel), a 1D scattered profile projection along the 2θ can be extracted. This procedure allows discrimination of signals from each individual crystallized and/or amorphous phase. We have also developed a reconstruction scheme that allows us to image the

stress distribution in crystalline phases by using the difference in 2θ position (lattice d spacing) and use it here to demonstrate residual stresses in the diamond core of the sample.

During our C_{60} to diamond experiment, we recovered a short interlayer disordered phase with $d_{00l} = 3.09\text{--}3.11 \text{ \AA}$, similar to those previously reported. The DSCT analysis provided evidence for the concentric spatial arrangement of this minor layered phase together with sp^3 -amorphous carbon and polycrystalline cubic diamond. This particular spatial arrangement is likely to be a consequence of the pressure gradient imposed by the anvil symmetry. The short c axis supports residual stresses in the sample, a phenomenon that is also corroborated by stress mapping of the polycrystalline diamond phase.

Figure 1(a) shows the 3D-DSCT phase distribution map. The sensitivity of this technique allowed for the identification of one crystalline phase and of three disordered phases, in contrast with standard diffraction experiment where only crystalline and amorphous diamond have been observed. The analysis of each slice [Fig. 1(b)] demonstrates that these phases exhibit concentric spatial arrangements similar to those reported by T. Ferroir *et al.* [23].

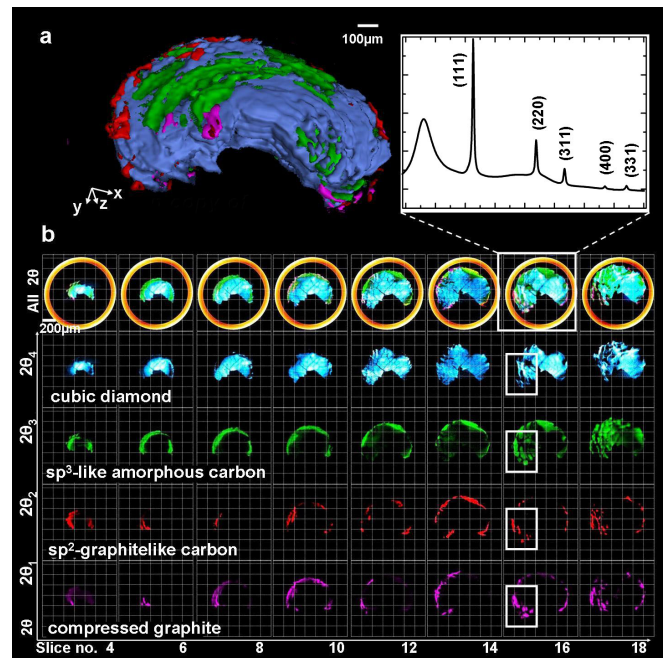


FIG. 1 (color online). (a) 3D-DSCT image of polycrystalline cubic diamond, sp^3 -like amorphous carbon, sp^2 -graphitelike, compressed graphite and quartz capillary. Voxel resolution is $6.6 \mu\text{m} \times 6.6 \mu\text{m} \times 8.0 \mu\text{m} \times 0.067^\circ$ ($x \times y \times z \times 2\theta$). (b) 2D-DSCT slices for each phase and their evolution with sample height (slice no.) for the full 2θ range, and for representative d spacing ($2\theta_i$). For slice no. 16, squares indicate the region of interest plotted in Fig. 2 and the inset shows the 1D scattering pattern for the summed contributions of all phases.

The sample core is made of polycrystalline diamond surrounded by an intermediate shell of sp^3 -like amorphous carbon and two different disordered carbon phases with $d_{00l} = 3.09\text{--}3.11$ Å and $d_{00l} = 3.35\text{--}3.42$ Å respectively. It should be noted that the latter may differ from sp^2 -like phases derived from the high-temperature treatment of C_{60} polymers. It is worth mentioning that for any untransformed C_{60} precursor at least three important reflections from remaining fcc structure or polymerized C_{60} would be expected. We did not observe these diffraction signals within the detection limits of our analysis (0.1% in volume).

In Fig. 2 we present the detailed analysis of a single sample slice (no. 16). For each phase, selective 1D scattered patterns are extracted and a region of interest close to the outermost shell of the sample is enlarged [Fig. 2(b), corresponding to the white rectangles drawn in Fig. 1(b)]. We observe the coexistence of the sp^2 -graphitelike phase (G) ($d_{00l} \sim 3.35\text{--}3.42$ Å) and the “compressed graphite” (CG) ($d_{00l} \sim 3.09\text{--}3.11$ Å) with the sp^3 -like amorphous phase.

This latter phase exhibits only two broad peaks at 2.12 and 1.22 Å; the same two homothetic broad peaks were reported for sp^3 -amorphous a -Si and a -Ge [29]. This amorphous phase can be simulated with sp^3 carbon models which contain mainly puckered sixfold rings of carbon having both “chair” and “boat” configurations [30]. These three poorly-ordered phases can coexist within the same diffracting volume. The d -spacing difference between G and CG phases, observed using DSCT, is confirmed on 2D microdiffraction or scattering patterns collected on selected mixed phase areas (Fig. 3). Additionally, both G and CG phases are textured, with a [001] preferential orientation. There is an offset between the texture directions of G phase and CG phase, the latter one being preferentially aligned parallel to the compression axis.

For all available sample orientations, no $(hk0)$ reflections are observed, supporting interlayer disorder. The elongated broad diffraction peaks also indicate some possible buckling of these layers. For the G phase, the interlayer distance is close to graphite ($d_{002\text{Graphite}} = 3.354$ Å), but for the CG phase this value is much smaller and can be explained either by residual stress or by the formation of C—C bonds between layers. From the d spacing of CG and from hydrostatic compressibility data of graphite [18] we estimate a residual pressure of ~ 5 GPa, suggesting that the polycrystalline diamond core could also contain some residual stress. As interlayer C—C bonds are unlikely to form without the application of HT they are likely to be the remnants of the C_{60} precursor. From these structural observations, we propose that this phase should no longer be associated to a graphitic structure.

Figure 4 highlights the polycrystalline cubic diamond phase. Images of slice no. 16 are extracted from different d spacing close to the (311) diamond reflection. The sample

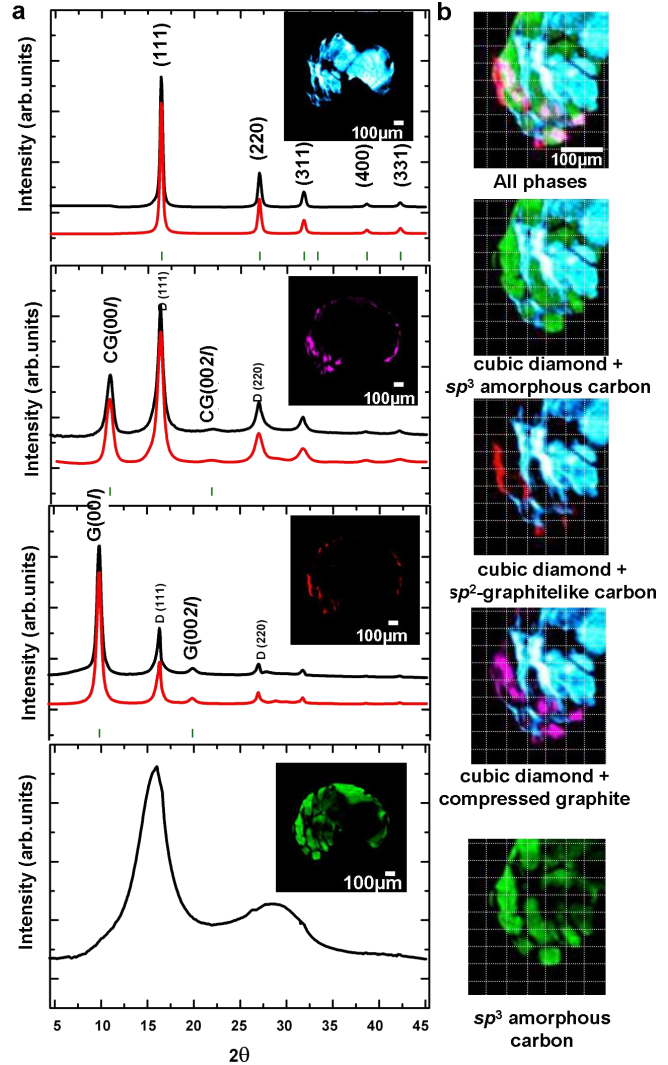


FIG. 2 (color online). Spatial phase-selective scattering analysis of slice no. 16. (a) 1D projected patterns (top) and Rietveld calculations (bottom) for cubic diamond $Fd\bar{3}m$ with $a = 3.565(1)$ Å, compressed graphite (CG) with $d_{00l} = 3.114(1)$ Å, sp^2 -graphitelike (G) with $d_{00l} = 3.420(1)$ Å and sp^3 -like amorphous carbon with 2.12 and 1.22 Å broad peaks. (b) Zoom on a region of interest (corresponding to white rectangles of Fig. 1) showing phase coexistence and interpenetrating morphology in the outer shell of the sample.

core consists of aggregates of diamond crystallites, with a fractured microstructure possibly due to a stress energy release event (also observed by electron microscopy on a similar sample). To check the strain in the diamond core we have also selected some volumes of interest to extract 1D patterns and estimated local lattice parameters and crystallite sizes from the (311) diamond reflection. Crystallite sizes vary from 6 to 10 nm, the smallest being in regions where cubic diamond and sp^3 -like amorphous carbon coexist. Cubic lattice parameters vary between 3.56 and 3.59 Å, indicating that the sample is composed of different domains having different lattice strain. This result was

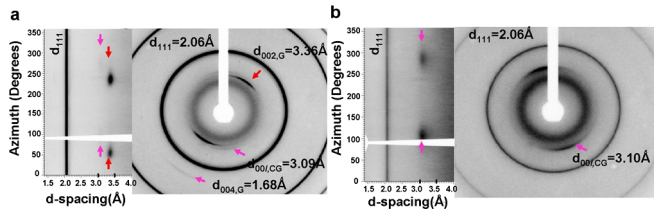


FIG. 3 (color online). Unrolled and 2D experimental microdiffraction or scattering pattern, collected from areas with high poly (a) morphous content, show 001 preferential orientation for (a) sp^2 -graphitelike phase (G) and “compressed graphite” (CG), (b) “compressed graphite” CG, evidencing their texture characteristics.

corroborated by identical maps obtained by using (111), (220), (400), or (331) cubic diamond reflections confirming that this is a direct sample characteristic and not due to sample-detector misalignments.

Performing the first 3D-DSCT selective mapping of disordered-heterogeneous materials, we demonstrate that CG can be recovered from C_{60} after room temperature compression. This CG phase was not associated to the presence of crystalline hexagonal diamond (HD) but to a sp^3 -like amorphous phase, even if we cannot exclude the presence of the HD phase at HP-HT conditions. The spatial repartition between CG and sp^3 -like amorphous phase is similar to the observation of CG crystallites hosted by HD crystallites by F.P. Bundy and J.S. Kasper [18] and the shell-like spatial arrangements is in agreement with the observations of C. Le Guillou *et al.* [3] and T. Ferroir *et al.* [23].

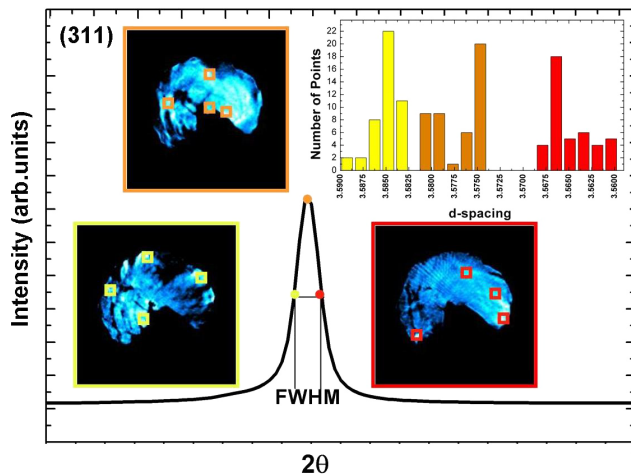


FIG. 4 (color online). 2D (x, y) lattice d -spacing maps of cubic diamond phase obtained at three different 2θ positions close to the (311) cubic diamond reflection: low-FWHM, center-FWHM, high-FWHM. As instrumental broadening gives rise to peak overlaps for data coming from different d -spacing areas, contrast in the image-reconstructions was enhanced by subtracting 20% of the center contribution. The squares indicate the zones of the sample that were used to extract 1D scattering patterns to build a histogram of lattice d -spacing distribution.

From our DSCT results and referring to current literature, possible transformation paths for C_{60} to diamond and graphite can be discussed. The P - T phase diagram of C_{60} is not yet fully understood, particularly in the high P - T area where C_{60} molecules and polymeric cages collapse. These corresponding sample signals are either featureless [31–33] or can exhibit a large variety in signature due to heterogeneity or small change in P - T -stress conditions [34,35]. Using DSCT we discriminate carbon phases based on slight variations of their scattering signal, and resolve the 3D heterogeneity of this phase transformation. The different localization of the phases G and CG support that they are structurally different and do not correspond to a continuous structure evolution of a sp^2 -graphitelike phase with a continuous shortening of interlayer spacing. The present CG synthesis process, which does not require the application of temperature, indicates that this phase differs from sp^2 -like phases derived from high-temperature treatment of C_{60} polymers. Both texture and reflection shapes of this CG phase [only (00 l) and (002 l) are observed] and their corresponding longer interlayer distance ($d_{00l} = 3.09$ – 3.11 Å) supports that this *quenched* CG phase is different from the superhard compressed graphite phase reported by W. Mao *et al.* [21]. It is more likely a phase closer to CG traces found in the presence of the major CD and HD phases reported by T. Irifune *et al.* [22] and to the CG phase found on a shocked meteorite by T. Ferroir *et al.* [23].

The nonhydrostatic pressurization treatment (i.e., induced stress) favors the C_{60} transformation into a sp^3 -like amorphous phase which contains also some mixture of sp^2 - sp^3 hybridized atoms. Simulations show that nonhydrostatic conditions lower the critical pressure for molecule collapse and increase the speed of this phase transformation [17]. Our structural maps do not show coexistence of both sp^2 -like phases (G and CG) with crystallized cubic diamond (CD). On the contrary, we found that the sp^3 -like amorphous phase is at the boundary of, on one side, the CD phase and, on the other, to the G and CG phases. There is also a clear coexistence of the CG phase and sp^3 -like amorphous phase. As we have studied a *quenched* sample, the transformation path probably involves this sp^3 -like amorphous phase.

Several possibilities of diamond nucleation or growth from graphite have been given. T. Irifune *et al.* [22] reported that at high pressure and temperatures: (i) above 2000 °C only CD is obtained and (ii) between 1800 and 2000 °C both CD and HD are recovered with the presence of a small amount of CG, $d_{00l} \sim 3.15$ Å. Starting from different carbon precursors, C. Le Guillou *et al.* [3] also reported that at 15 GPa and high temperature: (i) disordered precursors react faster than crystalline ones, (ii) quasiamorphous soot transforms to CD without prior graphitization process, (iii) highly oriented pyrolytic graphite mostly transforms into HD rather than CD. Our

maps also suggest that, starting from C_{60} molecules, under pressure stress and without external heating, CD could nucleate from the sp^3 -like amorphous phase. The single broad peak of this sp^3 disordered phase at 1.22 Å supports the presence of both chair and boat carbon rings, the first ones occurring in CD and both occurring in HD structure. These findings illustrate the necessity for further theoretical studies to explain this experimental observation and clarify the transition mechanism.

With the DSCT probe, we provide 3D phase distribution maps showing shell-like arrangements of cubic diamond, sp^3 -like amorphous carbon, sp^2 -graphitelike carbon, and so-called “compressed graphite.” In addition, we demonstrate that scattering contrast is key in discriminating between polyamorph-polycrystalline heterogeneous phases, especially when the similarities in phase densities or when weak signals of amorphous systems limit the use of other methods. The use and sensitivity of this probe for strain contrast is clearly demonstrated for crystalline diamond in this Letter, and therefore could be applied for materials with smaller bulk modulus values. The DSCT analysis strategy presented here allows the reconstruction of the first 3D real space image (spatial phase-selective resolution) of a heterogeneous sample and gives access to the reciprocal space information (structural resolution) simultaneously.

The authors wish to acknowledge M. Núñez-Regueiro, G. Renaud, P. Launois, L. Marques, S. Petitgirard, D. Testemale, and R. Tucoulou for manuscript comments and discussions and M.N-R for sample synthesis. The European Synchrotron Radiation Facility is acknowledged for provision of the synchrotron radiation beam. M. A. acknowledges CONACYT Grant No. 211996.

*Corresponding author: hodeau@grenoble.cnrs.fr

- [1] see as example: T. Teraji, *Phys. Status Solidi A* **203**, 3324 (2006); J. Robertson, *Mater. Sci. Eng. R* **37**, 129 (2002); F.P. Bundy, W.A. Bassett, M.S. Weathers, R.J. Hemley, H.U. Mao, A.F. Goncharov, *Carbon* **34**, 141 (1996); T. Irifune, A. Kurio, S. Sakamoto, T. Inoue, and H. Sumiya, *Nature (London)* **421**, 599 (2003).
- [2] see as example: R.Z. Khaliullin, H. Eshet, T.D. Kühne, J. Behler, and M. Parrinello, *Nature Mater.* **10**, 693 (2011).
- [3] C. Le Guillou, F. Brunet, T. Irifune, H. Ohfuji, J.-N. Rouzaud, *Carbon* **45**, 636 (2007).
- [4] K. Niwase, K.G. Nakamura, M. Yokoo, K.-I. Kondo, and T. Iwata, *Phys. Rev. Lett.* **102**, 116803 (2009).
- [5] B. Sundqvist, *Adv. Phys.* **48**, 1 (1999).
- [6] V.D. Blank, S.G. Buga, G.A. Dubitsky, N.R. Serebryanaya, M. Yu. Popov, B. Sundqvist, *Carbon* **36**, 319 (1998).
- [7] E.V. Tat'yanin, A.G. Lyapin, V.V. Mukhamadiarov, V.V. Brazhkin, and A.L. Vasiliev, *J. Phys. Condens. Matter* **17**, 249 (2005).
- [8] R. Moret, *Acta Crystallogr. Sect. A* **61**, 62 (2004).
- [9] V.D. Blank, B.A. Kulnitskiy, and Ye. V. Tatyani, *Phys. Lett. A* **204**, 151 (1995).
- [10] S.J. Duclos, K. Brister, R.C. Haddon, A.R. Kortan, and F.A. Thiel, *Nature (London)* **351**, 380 (1991).
- [11] M. Núñez-Regueiro, P. Monceau, and J.L. Hodeau, *Nature (London)* **355**, 237 (1992).
- [12] M. Núñez-Regueiro, P. Monceau, A. Rassat, P. Bernier, and A. Zahab, *Nature (London)* **354**, 289 (1991).
- [13] F. Moshary, N.H. Chen, I. Silvera, C.A. Brown, H.C. Dorn, M.S. de Vries, and D.S. Bethune, *Phys. Rev. Lett.* **69**, 466 (1992).
- [14] L. Zeger and E. Kaxiras, *Phys. Rev. Lett.* **70**, 2920 (1993).
- [15] B.L. Zhang, C.Z. Wang, K.M. Ho, and C.T. Chan, *Europhys. Lett.* **28**, 219 (1994).
- [16] H. Hirai, K. Kondo, and T. Ohwada, *Carbon* **31**, 1095 (1993).
- [17] M. Moseler, H. Riedel, P. Gumbsch, J. Stäring, and B. Mehlh, *Phys. Rev. Lett.* **94**, 165503 (2005).
- [18] F.P. Bundy and J.S. Kasper, *J. Chem. Phys.* **46**, 3437 (1967).
- [19] Y.X. Zhao and I.L. Spain, *Phys. Rev. B* **40**, 993 (1989).
- [20] T. Yagi, W. Utsumi, M.-A. Yamakata, T. Kikegawa, and O. Shimomura, *Phys. Rev. B* **46**, 6031 (1992).
- [21] W.L. Mao, H.-k. Mao, P.J. Eng, T.P. Trainor, M. Newville, C.-c. Kao, D.L. Heinz, J. Shu, Y. Meng, and R.J. Hemley, *Science* **302**, 425 (2003).
- [22] T. Irifune, A. Kurio, S. Sakamoto, T. Inoue, H. Sumiya, and K. Funakoshi, *Phys. Earth Planet. Inter.* **143–144**, 593 (2004).
- [23] T. Ferroir, L. Dubrovinsky, A. El Goresy, A. Simionovici, T. Nakamura, and P. Gillet, *Earth Planet. Sci. Lett.* **290**, 150 (2010).
- [24] M. Amsler *et al.*, *Phys. Rev. Lett.* **108**, 065501 (2012).
- [25] P. Bleuet, E. Welcomme, E. Dooryhée, J. Susini, J.-L. Hodeau, and P. Walter, *Nature Mater.* **7**, 468 (2008).
- [26] S.R. Stock, F. De Carlo, and J.D. Almer, *J. Struct. Biol.* **161**, 144 (2008).
- [27] M. Álvarez-Murga, P. Bleuet, L. Marques, C. Lepoittevin, N. Boudet, G. Gabarino, M. Mezouar and J.-L. Hodeau, *J. Appl. Crystallogr.* **44**, 163 (2010) and references therein.
- [28] S.D.M. Jacques, M. Di Michiel, A.M. Beale, T. Sochi, M.G. O'Brien, L. Espinosa-Alonso, B.M. Weckhuysen, P. Barnes, *Angew. Chem., Int. Ed. Engl.* **50**, 10148 (2011).
- [29] A.C. Wright, A.C. Hannon, R.N. Sinclair, T.M. Brunier, C.A. Guy, R.J. Stewart, M.B. Strobel, and F. Jansen, *J. Phys. Condens. Matter* **19**, 415109 (2007).
- [30] J.L. Hodeau, J.M. Tonnerre, B. Bouchet-Fabre, M. Núñez Regueiro, J.J. Capponi, and M. Perroux, *Phys. Rev. B* **50**, 10311 (1994).
- [31] A.V. Talyzin, L.S. Dubrovinsky, T. Le Bihan, and U. Jansson, *J. Chem. Phys.* **116**, 2166 (2002).
- [32] A.V. Talyzin, and L.S. Dubrovinsky, *Phys. Rev. B* **68**, 233207 (2003).
- [33] A. Dzwilewski, A. Talyzin, G. Bromiley, S. Dub, and L. Dubrovinsky, *Diam. Relat. Mater.* **16**, 1550 (2007).
- [34] V.D. Blank, S.G. Buga, N.R. Serebryanaya, V.N. Denisov, G.A. Dubitsky, A.N. Ivlev, B.N. Mavrin, and M. Yu. Popov, *Phys. Lett. A* **205**, 208 (1995).
- [35] A.V. Talyzin, F. Langenhorst, N. Dubrovinskaia, S. Dub, and L.S. Dubrovinsky, *Phys. Rev. B* **71**, 115424 (2005).